C. R. Chimie 19 (2016) 1310–1314

Contents lists available at ScienceDirect

Comptes Rendus Chimie

www.sciencedirect.com

Preliminary communication/Communication

Resonance Raman spectroscopy as a probe of the crystallite size of MoS_2 nanoparticles

Élodie Blanco [a], Pavel Afanasiev [a], Gilles Berhault [a], Denis Uzio [b], Stéphane Loridant [a, *]

[a] IRCELYON, CNRS, University of Lyon 1, 2, av. Albert-Einstein, 69626 Villeurbanne, France
[b] IFP Énergies Nouvelles, rond-point de l'Échangeur de Solaize, BP 3, 69360 Solaize, France

ARTICLE INFO

Article history:
Received 26 June 2015
Accepted 28 August 2015
Available online 2 March 2016

Keywords:
MoS_2
Resonance Raman spectroscopy
Crystallite size
Nanoparticles
Inorganic fullerene

ABSTRACT

Irregularly shaped and inorganic fullerene-like MoS_2 compounds were characterized by Resonance Raman spectroscopy using an exciting line at 633 nm. It was shown that the relative intensity of the longitudinal acoustic mode at 226 cm^{-1} and its overtone strongly depends on the MoS_2 crystallite size but not on the size of the particles made of agglomerated crystallites. This technique appeared as a promising probe to characterize *in situ* very small crystallites that are not observed by XRD.

1. Introduction

Molybdenum disulfide MoS_2 is an important inorganic material mainly studied as a heterogeneous catalysts, electrocatalysts, photocatalysts, lubricants, anode materials for Li-ion batteries, photoluminescent material, and polymer composites [1]. For all these applications, particular properties can be obtained at the nano-scale level and therefore structural characterization of MoS_2 nanostructures is required.

In the literature, non-resonant Raman spectroscopy has been widely used to characterize MoS_2 thin films. In particular, the dependence of the A_{1g} and E_{2g} vibrational modes was investigated depending on the number of MoS_2 layers [2–5], on interaction with a sapphire or SiO_2 substrate [6,7] or for probing van der Waals forces acting between two atomically thin crystals [8]. For nanocrystallized MoS_2 films, additional Raman modes associated with the folding of the Brillouin zone along certain directions were observed in comparison to bulk MoS_2 [9] but their application was limited due to small inherent intensity.

The resonance Raman effect is a particular case of Raman scattering taking place when the wavelength of the exciting line is in resonance with the electronic absorption of the sample: the vibrations involved in the electronic transition are then strongly enhanced [10,11]. Hence, the use of resonance conditions allows probing both changes of structural and electronic states.

The Raman and resonance Raman spectra of MoS_2 nanoparticles were compared in previous studies [12,13]: using resonance conditions, several additional first-order and enhanced second order bands were observed. Some of them corresponding to phonons in the vicinity of the Brillouin zone edge are believed to be disorder induced [13]. Therefore, resonance Raman spectroscopy can be used to detect structural defects or conversely to check for a good crystallinity as it was done for MoS_2 nanotubes [14]. Furthermore, a relationship between the intensity ratio of the bands at 455 and 465 cm^{-1} and the particle size was established [13,15]. In another study, this ratio was shown

* Corresponding author.
E-mail address: stephane.loridant@ircelyon.univ-lyon1.fr (S. Loridant).

http://dx.doi.org/10.1016/j.crci.2015.08.014

to increase by decreasing the number of MoS_2 layers [5]. However, most phonon modes are significantly broadened or strongly suppressed in single-layer MoS_2 under resonance conditions [12].

In this work, two series of fullerene like (IF) MoS_2 issued from core shell ZnS@MoS_2 preparation and irregularly shaped MoS_2 particles (ex ammonium thiomolybdate, ATM) have been characterized by resonance Raman spectroscopy after sulphidation at different temperatures. The main enquiry was on the presence and origin of morphology induced particular features of Raman spectra.

2. Experimental part

The preparation of fullerene-like MoS_2 by thermal decomposition of ammonium tetrathiomolybdate, $(NH_4)_2MoS_4$, (ATM) has been previously described [16]. ATM dark red crystals were obtained by addition of 15 g of $(NH_4)_6Mo_7O_{24}\cdot 4H_2O$ to 200 mL of a 20 wt% solution of $(NH_4)_2S$ upon stirring at ambient temperature. The precipitate was filtered off, washed with ethanol, and dried. ATM was decomposed under a H_2S/H_2 (15% v/v in H_2S) flow at different temperatures. These compounds are labeled MoS_2-ATM-T where *T* corresponds to the decomposition temperature.

The preparation of core shell ZnS@MoS_2 solids has been detailed elsewhere [1]. Briefly, two solutions pre-heated at 180 °C in ethylene glycol (EG), one of ammonium heptamolybdate and the other one containing ZnS seed, were added to a boiling EG solution of elemental sulfur. The Zn/Mo molar ratio was fixed at 1. The brown powder obtained after 1 h at reflux was then separated and thermally treated under H_2S/H_2 (8% vol in H_2S) at different temperatures. These compounds that corresponded to fullerene-like compounds [1] are labeled MoS_2-IF-T where *T* corresponds to the decomposition temperature.

Transmission Electron Microscopy (TEM) was carried out on a JEOL 2010 device with an accelerating voltage of 200 keV. The samples were dispersed in n-hexane by using ultrasound, and then put onto a porous carbon filament on a copper grid sample holder. In order to protect them from oxidation by air, the samples still covered with liquid hexane were immediately introduced into the TEM vacuum chamber.

The X-ray diffraction (XRD) patterns were obtained on a Bruker diffractometer with Cu Kα emission and identified using standard ICDD files. The mean crystallite size was determined using the Scherrer equation: $D_{110} = \frac{k_{110}\lambda}{\beta_{110}\cos\theta}$ where D_{110} is the dimension of the platelet, λ is the wavelength of X-rays, Θ is the diffraction angle near 14° (2Θ) and β_{110} (or FWHM) is the angular line width. The shape factor k_{110} was equal to 1.32 [17,18]. The mean stacking along the c direction was calculated from a similar equation: $D_{002} = \frac{k_{002}\lambda}{\beta_{002}\cos\theta}$ where D_{002} is the crystallite dimension along the *c* direction, λ is the wavelength of X-rays, Θ is the diffraction angle near 59–60° (2Θ) and β_{002} (or FWHM) is the angular line width. The shape factor k_{002} was equal to 0.76 [17,18].

Raman spectra were recorded with a LabRam HR Raman spectrometer (Horiba-Jobin Yvon) equipped with a BXFM confocal microscope, interference and edge filters and a charge-coupled device detector. The exciting line of an Ar^+ ion laser at 514.5 nm or a He–Ne laser at 632.8 nm was focused using a ×50 long working distance objective. The backscattered light was dispersed with a grating of 1800 grooves mm^{-1} providing a spectral resolution of 1 cm^{-1}. The position of bands was previously calibrated from the 521 cm^{-1} band of the Si plate.

3. Results

The fullerene-like MoS_2 compounds contained a ZnS phase as an impurity in the form of large (micron-size) crystallites, present due to the preparation technique. In both the cases of MoS_2-IF and MoS_2-ATM, increasing the treatment temperature was shown to favor the MoS_2 crystalline growth and closure of the slabs [1,16], whereas the size of particles made by the stacking of MoS_2 slabs did not vary strongly as shown in TEM images (Fig. 1).

The comparison of the Raman spectra of MoS_2-IF-750 achieved with different exciting lines (Fig. 2) confirmed that mainly the E_{2g} and A_{1g} modes at 384 and 408 cm^{-1}, respectively [13,19] are observed using non-resonant conditions (514.5 nm). The E_{1g} mode near 285 cm^{-1} (Fig. 2) is also Raman active in bulk 2H MoS_2 because it is located at the Γ point in the hexagonal Brillouin zone [13,19]. As this mode is forbidden in backscattering experiments on a surface perpendicular to the *c* axis [13], its observation revealed that the MoS_2 layers were not perpendicular to the laser but were randomly oriented (no polarization effect).

Additional bands were observed using resonant conditions (632.8 nm). These bands were not due to ZnS since its main band located at 348 cm^{-1} [20] was not observed. Hence, micron-size standalone ZnS crystallites do not interfere with Raman observations of MoS_2. Table 1 gathers the assignments of the observed MoS_2 Raman bands from the literature [13,15,21,22]. The band at 227 cm^{-1} was proposed to be induced by disorder similar to nanocrystallized graphite or SiC [23,24] and corresponds to a longitudinal acoustic mode (LA) located at the M point of the Brillouin zone [13]. This mode observed at 514.5 nm (Fig. 2) would be enhanced at 632.8 nm because of the modification of the electronic band structure of small particles leading to higher resonance. Note that the LA(M) mode was not observed under resonance conditions for MoS_2 nanoparticles [15] and was very weak for few layer MoS_2 [5]. It is clearly evidenced that resonance conditions are not enough to observe the band at 226 cm^{-1} with high relative intensity. The second order band at 419 cm^{-1} depends on the electronic state of MoS_2 [13,25] as well as the A_{2u} mode at 468 cm^{-1} which is only IR active under non-resonant conditions [13]. Finally, the bands at higher wavenumbers were attributed to combinations or overtones. In particular, the band at 453 cm^{-1} corresponds to the overtone of the one at 226 cm^{-1} (2 × LA(M)) and is enhanced under resonance conditions by coupling to electronic transitions associated with the excitonic states [26].

The resonance Raman spectra of the MoS_2-ATM and MoS_2-IF series are compared in Fig. 3. The wavenumbers of the A_{1g} and E_{2g} modes were close to the bulk ones [3,18] for

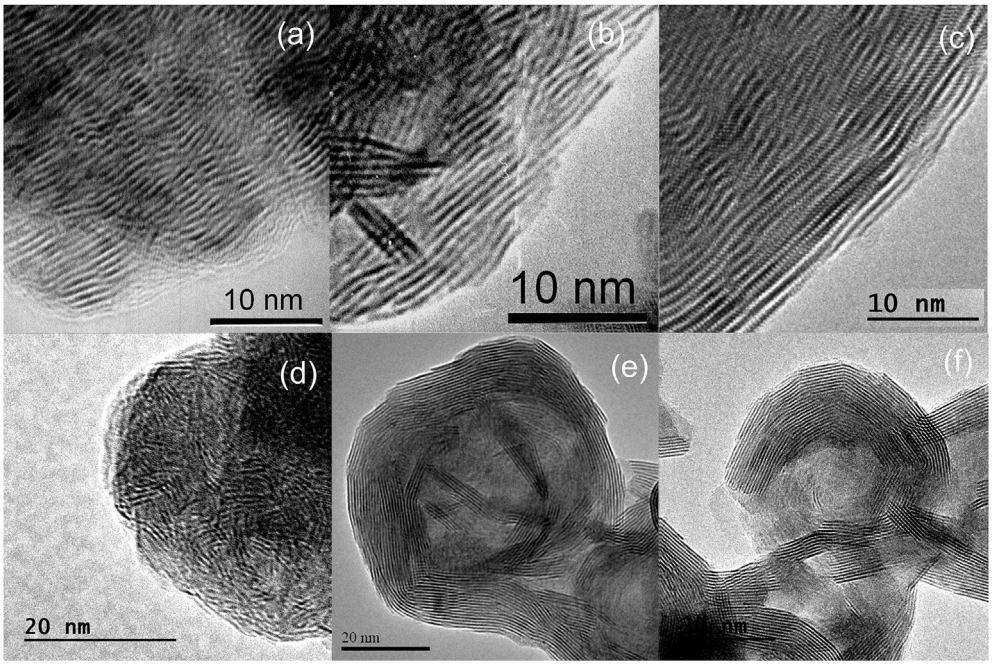

Fig. 1. TEM images of (a) MoS_2-ATM-400, (b) MoS_2-ATM-550, (c) MoS_2-ATM-750, (d) MoS_2-IF-400, (e) MoS_2-IF-550 and (f) MoS_2-IF-750.

MoS_2-ATM-750 and MoS_2-IF-750 (385 and 408 cm^{-1}, respectively). However, they were red-shifted for the others. The effect of the laser has to be ruled out since it was negligible for the power value used (100 μW). Furthermore, similar red-shifts were previously observed for MoS_2-IF samples [13,15]. They cannot also arise from low stacking since it was equal to 5.1 for MoS_2-ATM-400 and higher than 6 for the other samples. One can notice that the relationship between the wavenumber difference $\Delta\omega(A_{1g}-E_{2g})$ and the N stacking value ($\Delta\omega(A_{1g}-E_{2g}) = 25.8-8.4/N$) established for MoS_2 large layers [3] does not work in our case. As an out-of-plane strain induces a blue-shift of the two bands, like that for MoS_2 nanotubes [14,27], such explanation was also ruled out. In fact, the red-shifts could be explained by in-plane compressive strains [27] between small MoS_2 platelets agglomerated in particles.

Fig. 3 also evidences that the high relative intensity of the bands at 228 and 456 cm^{-1} is not specific to small

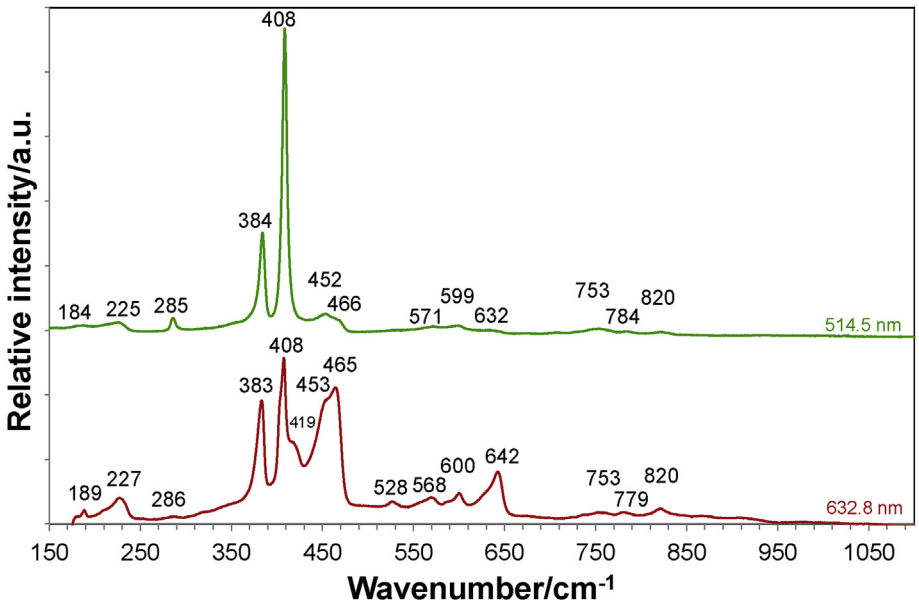

Fig. 2. Comparison of non-resonant (514.5 nm) and resonant (632.8 nm) Raman spectra of the MoS_2-IF-750 sample.

Table 1
Assignments of MoS_2 Raman bands.

Wavenumber (cm^{-1})	Assignment
189	A_{1g}(M)-LA(M)
227	LA (M)
285	$E_{1g}(\Gamma)$
384	$E_{2g}(\Gamma)$
408	$A_{1g}(\Gamma)$
419	$B_{2g} + E_{1u}(\Gamma$-A)
453	2 × LA(M)
468	$A_{2u}(\Gamma)$
528	$E_1g(M)$ + LA(M)
568	2 × $E_{1g}(\Gamma)$
600	E_{2g}(M) + LA(M)
642	A_{1g}(M) + LA(M)

fullerene-like MoS_2 compounds. It is also important to notice that the band at 495 cm^{-1}, claimed to be typical of fullerenes [28], has not been observed in the present study. However, the spectrum of MoS_2-ATM-400 contained a small band at 483 cm^{-1} that could be attributed to the presence of defects [13] possibly located at the grain boundary. Furthermore, MoS_2-IF-550 and MoS_2-IF-750 exhibited very different relative intensities of the bands at

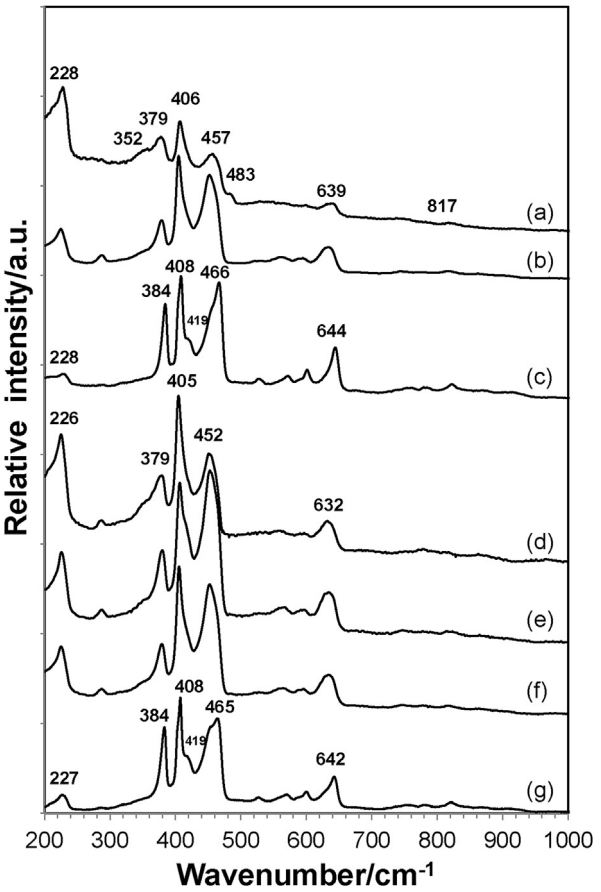

Fig. 3. Raman spectra of (a) MoS_2-ATM-400, (b) MoS_2-ATM-550, (c) MoS_2-ATM-750, (d) MoS_2-IF-400, (e) MoS_2-IF-500, (f) MoS_2-IF-600, and (g) MoS_2-IF-750.

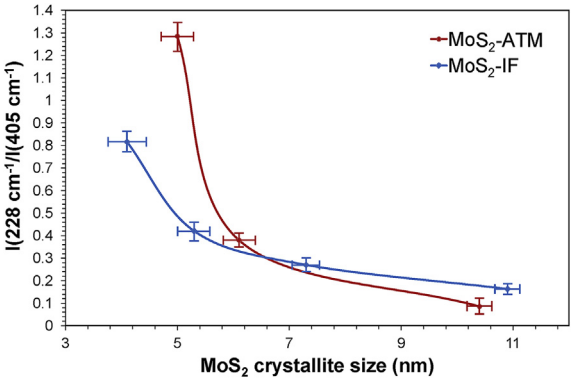

Fig. 4. Evolution of the I(228 cm^{-1})/I(405 cm^{-1}) intensity ratio versus the MoS_2 crystallite size deduced from the (110) XRD band.

228 and 456 cm^{-1} in spite of similar particle sizes (Fig. 1). Hence, the particle size appeared to be a parameter not determining their relative intensities. Furthermore, it clearly appeared that they strongly diminished with the sulphidation temperature (Fig. 3). As the crystallite size strongly increased with the sulphidation temperature [1,16], the relative intensity of the band at 228 cm^{-1} was plotted as a function of this parameter deduced from XRD (Fig. 4): a clear decreasing correlation was established for the first time. It showed that this parameter was the key contrarily to the particle size. However, it is influenced by another parameter since an intensity ratio of 1.28 was determined for MoS_2-ATM-400 at ca 5 nm instead of 0.42 for MoS_2-IF-500 samples having the same crystallite size. Considering that relative intensity of the band at 228 cm^{-1} (and of its overtone) is influenced at low stacking [5], the higher intensity observed for MoS_2-ATM-400 could arise from a mean stacking of only 5.1. The influence of the stacking could be negligible otherwise since this parameter was equal to 6.5 for MoS_2-IF-400 and higher than 7.5 for the other samples.

4. Conclusion

As a conclusion, resonance Raman spectroscopy appeared as a powerful technique to probe the MoS_2 crystallite size from the relative intensity of the mode at 226 cm^{-1} activated under resonance conditions. It should be of particular interest for supported MoS_2 catalysts which contain very small crystallites that cannot be observed by X-ray diffraction or by standard transmission electron microscopy [29]. In particular, the MoS_2 dispersion could be evaluated *in situ* by this technique [30].

References

[1] E. Blanco, D. Uzio, G. Berhault, P. Afanasiev, J. Mater. Chem. A 2 (2014) 3325–3331.
[2] C. Lee, H. Yan, L.E. Brus, T.F. Heinz, J. Hone, S. Ryu, ACS Nano 4 (2010) 2695–2700.
[3] X. Zhang, X.-F. Qiao, W. Shi, J.-B. Wu, D.-S. Jiang, P.-H. Tan, Chem. Soc. Rev. 44 (2015) 2757–2785.
[4] J. Tao, J. Chai, X. Lu, L.M. Wong, T.I. Wong, J. Pan, Q. Xiong, D. Chi, S. Wang, Nanoscale 7 (2015) 2497–2503.

[5] B. Chakraborty, H.S.S. Ramakrishna Matte, A.K. Sood, C.;N.R. Rao, J. Raman Spectrosc. 44 (2013) 92–96.
[6] H. Liu, A.K.K. Antwi, J. Ying, S. Chua, D. Chi, Nanotechnology 25 (2014) 405702.
[7] L. Su, Y. Zhang, Y. Yu, L. Cao, Nanoscale 6 (2014) 4920–4927.
[8] K.-G. Zhou, F. Withers, Y. Cao, S. Hu, G. Yu, C. Casiraghi, ACS Nano 8 (2014) 9914–9924.
[9] A.P.S. Gaur, S. Sahoo, M. Ahmadi, M.J.-F. Guinel, S.K. Gupta, R. Pandey, S.K. Dey, R.S. Katiyar, J. Phys. Chem. C 117 (2013) 26262–26268.
[10] A. Myers Kelley, J. Phys. Chem. A 112 (2008) 11975–11991.
[11] P.C. Stair, Adv. Catal. 51 (2007) 75–98.
[12] J.-H. Fan, P. Gao, A.-M. Zhang, B.-R. Zhu, H.-L. Zeng, X.-D. Cui, R. He, Q.-M. Zhang, J. Appl. Phys. 115 (2014) 053527.
[13] G.L. Frey, R. Tenne, M.J. Matthews, M.S. Dresselhaus, G. Dresselhaus, Phys. Rev. B 60 (1999) 2883–2892.
[14] M. Virsek, A. Jesih, I. Milosevic, M. Damnjanovic, M. Remskar, Surf. Sci. 601 (2007) 2868–2872.
[15] H. Wu, R. Yang, B. Song, Q. Han, J. Li, Y. Zhang, Y. Fang, R. Tenne, C. Wang, ACS Nano 5 (2011) 1276–1281.
[16] P. Afanasiev, J. Catal. 269 (2010) 269–280.
[17] G. Berhault, M. Perez De la Rosa, A. Mehta, M.J. Yácaman, R.R. Chianelli, Appl. Catal., A 345 (2008) 80–88.
[18] K.S. Liang, R.R. Chianelli, F.Z. Chien, S.C. Moss, J. Non-Cryst. Solids 79 (1986) 251–273.
[19] M.P. Deshpande, S.V. Bhatt, V. Sathe, B.H. Soni, N. Garg, S.H. Chaki, in: Solid State Physics: Proceeding of the 57th Solid State Physics Symposium 2012, Mumbai, India, AIP Conf. Proceedings, vol. 1512, 2013, pp. 808–809.
[20] A. Fairbrother, V. Izquierdo-Roca, X. Fontané, M. Ibáñez, A. Cabot, E. Saucedo, A. Pérez-Rodríguezac, CrystEngComm 16 (2014) 4120–4125.
[21] K. Gołasa, M. Grzeszczyk, P. Leszczynski, C. Faugeras, A.A.L. Nicolet, A. Wysmołek, M. Potemski, A. Babinski, Appl. Phys. Lett. 104 (2014) 092106.
[22] J.M. Chen, C.S. Wang, Solid State Commun. 14 (1974) 857–860.
[23] G. Gouadec, P. Colomban, Prog. Cryst. Growth Charact. Mater 53 (2007) 1–56.
[24] S. Karlin, Ph. Colomban, J. Raman Spectrosc. 28 (1997) 219–228.
[25] T. Sekine, K. Uchinokura, T. Nakashizu, E. Matsuura, R. Yoshizaki, J. Phys. Soc. Jap. 53 (1984) 811–818.
[26] A.M. Stacy, D.T. Hodul, J. Phys. Chem. Solids 46 (1985) 405–409.
[27] L. Yang, X. Cui, J. Zhang, K. Wang, M. Shen, S. Zeng, S.A. Dayeh, L. Feng, B. Xiang, Scientific Rep. 4 (2014) 5649.
[28] M. Remskar, A. Mrzel, M. Virsek, A. Jesih, Adv. Mater. 19 (2007) 4276–4278.
[29] V.O. Koroteev, D.A. Bulushev, A.L. Chuvilin, A.V. Okotrub, L.G. Bulusheva, ACS Catal. 4 (2014) 3950–3956.
[30] C. Legens, P. Raybaud, in: H. Toulhoat, P. Raybaud (Eds.), Catalysis by Transition Metal Sulphides: From Molecular Theory to Industrial Application, Editions Technip, 2013, pp. 283–284.